===== From the Researcher's Notebook =====

The Main Statistical and Kinematic Properties of the Gaia EDR3 Catalog

A. S. Tsvetkov[#]

St. Petersburg State University, St. Petersburg, Russia
e-mail: a.s.tsvetkov@inbox.ru

Abstract—In a recent issue of the journal Herald of the RAS (No. 1, 2021), the article "Achievements of Space Astrometry" discussed the development of astrometry from ancient times to the Gaia space project. In this work, continuing this topic, the properties of the latest release of the Gaia EDR3 stellar catalog, containing 1.8 billion objects, are analyzed in detail. Methods of processing its data on personal computers accessible to most users are discussed. A detailed statistical study of the catalog was carried out, and the distribution of stars in the celestial sphere was obtained, making it possible to assess the volume and quality of the material. The analysis of the three-band photometry of the catalog is made, and the distributions of color indices and the Hertzsprung−Russell diagram are plotted.

The Gaia spacecraft is still in orbit, and the final catalog is planned for release in the first half of 2022 [1]. Preliminary catalogs have already been published: the so-called Data Release DR1 and DR2. On December 3, 2020, Gaia Early Data Release 3 [2] was released—an "early release of the final catalog" [2]. The method of its construction is described in detail in [3]. There are so many publications devoted to these data that even a brief listing of their names is not possible. The Gaia consortium has access to huge computing resources, distributed computing systems, and special laboratories with engineers and programmers. The question arises: is it possible with the help of more modest resources to conduct scientific research not only of small subsets of the catalog, such as TGAS [4] or Gaia DR2 with Radial Velocities [5], but of the entire data volume? Practice has shown that, with well-defined tasks, known optimization of computing processes, fast storage media, and modern personal computers with sufficient RAM, such work is quite possible and serves as a good preparation for processing the final version of the catalog (apparently, the first, since it is obvious that it will be further improved).

The quality of individual parallaxes in Gaia EDR3 is very far from predicted, so we carried out a series of standard studies already applied to mass catalogs, for example, NOMAD [6], which contains 1.1 bln objects, or PPMXL [7], 910 mln stars.

ORGANIZATION OF THE CATALOG

The source data of the EDR3 catalog are available on the official Gaia website as 3386 compressed files of about 200 MB each. When unpacking, the file size increases by about two times, up to 400−450 MB. Thus, the total amount of downloaded data is about 670 GB, and the unpacked data require storage of about 1.5 TB. The file format is CSV text, and the fields of each star are separated by commas. If any data is missing (and this is often the case), two commas appear in a row. This format of the initial data is easily supported by the FORTRAN language [8].

Each line contains information about 99 fields for one star. A detailed description of each field is given in [9]. The fields can be categorized as follows:

• identifiers;

• astrometric parameters: coordinates, proper motions, parallax, and their errors;

• correlations between parameters;

• number and quality of astrometric observations;

• photometry in three bands;

• radial velocities (from DR2);

• galactic and ecliptic coordinates.

It should be said that full reading of the catalog as text takes many hours. For stellar kinematic studies, not all fields are necessary; therefore, the first proce-

---

[#] Aleksandr Stanislavovich Tsvetkov, Cand. Sci. (Phys.−Math.), is an Associate Professor in the Department of Astronomy at St. Petersburg State University (SPbSU).
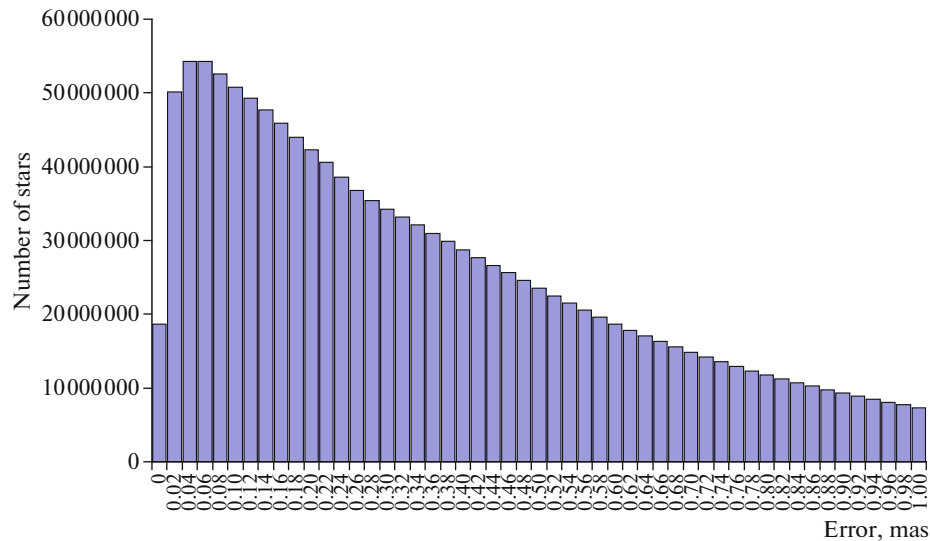
Fig. 1. Distribution of Gaia EDR3 stars by parallax error.

dure in processing such data is to extract the necessary information and write the data in binary form so as not to transform them during subsequent reading. The reformatting procedure, which really requires reading all the text data, is enough to carry out once. For our purposes, we chose 22 main fields, while the total amount of uncompressed binary data was reduced to 250 GB, and taking into account the capabilities of modern file systems to compress data dynamically (this increases the read speed: fewer blocks need to be read), the volume was only 180 GB. Placing such comparatively small data on a fast hard drive, or better on an SSD, leads to a significant increase in the speed of solving problems that require reading the entire catalog.

GENERAL STATISTICAL ANALYSIS

Before conducting any research, it is necessary to understand the accuracy, volume, and main features of the observational material. Although the Gaia website contains a lot of this kind of information, one should always repeat this research oneself to ensure that the entire computational process is correct.

Parallaxes. Gaia's most important planned result is highly accurate individual stellar parallaxes. Currently, the declared accuracy (0.01 mas, milliarcsecond) for most stars has not yet been achieved [10]. Parallax data in the catalog exist for 1 467 744 818 stars, while such data is absent for 343 964 953 stars. Figure 1 shows the distribution of stars by the absolute parallax error, expressed in mas. Analysis of this diagram shows that there is a large proportion of stars with errors of tenths of mas and higher. Only 500 million stars have an accuracy better than 0.2 mas, that is, about a third of those with parallax data. This leads to the distribution of stars according to the relative parallax error, as shown in Fig. 2. Approximately the same part (520 million) of stars have a relative parallax error of better than 50%; and only 98 million, less than 10%.

The most interesting result is the distribution of stars by parallaxes (Fig. 3). It can be seen that 283 million stars have a negative parallax, which contradicts the geometric meaning of the concept itself. At the same time, as detailed analysis shows, it is absolutely not necessary that such parallaxes have large root mean square errors. This fact suggests that the work on Gaia parallaxes still requires significant efforts and the establishment of an exact zero point for parallaxes.

Thus, individual parallaxes should be used with caution, although statistically, for large groups of stars, the averaged parallaxes give rather reliable results, which will be demonstrated by the example of constructing the Hertzsprung–Russell diagram.

Proper motions. All 1 811 709 771 stars without exception have data on the proper motions of $\mu_\alpha \cos \delta$ and μ_δ. The accuracies listed in the catalog in a random relation also have not yet reached the projected ones. Only 213 million stars have full accuracy of proper motion better than 0.1 mas/yr, and 406 million, better than 0.2 mas/yr. However, the relative accuracy of proper motions is much better than that of parallaxes, due to the fact that the proper motions themselves are greater than the parallax displacements (Fig. 4). The total proper motion of 77% of stars lies in the range from 2 to 8 mas/yr, and 93%, in the range from 0 to 10 mas/yr. Thus, almost half of the stars in the catalog have a relative accuracy of proper motions better than 10%. Such high accuracy allows any stellar kinematic studies based on the analysis of the proper motions of stars.
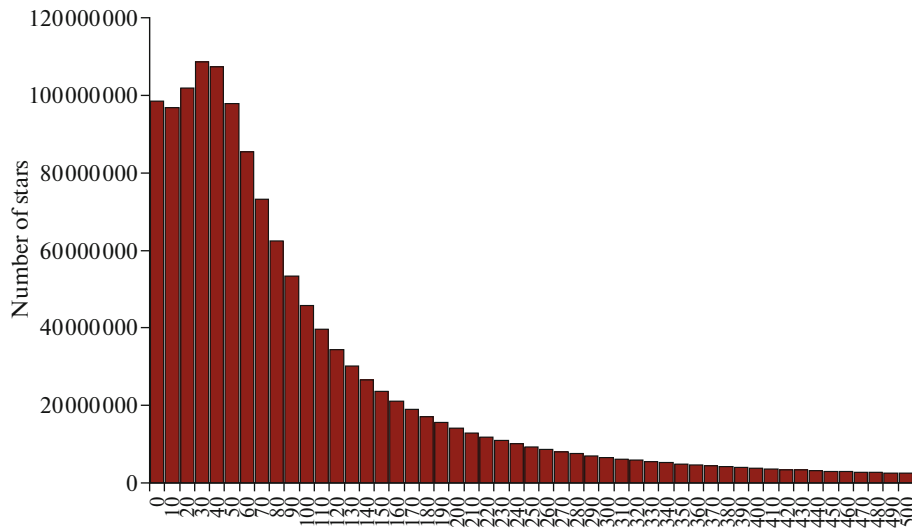
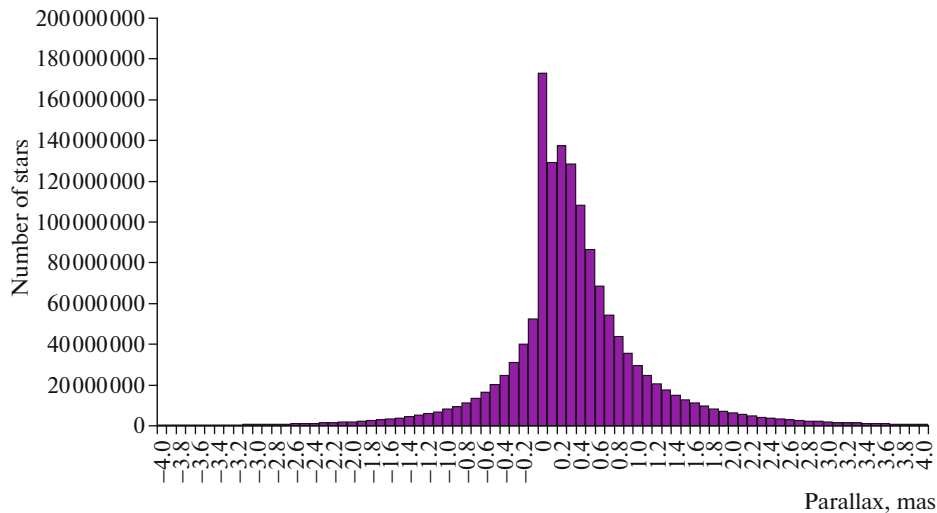**Fig. 2.** Distribution of Gaia EDR3 stars by the relative parallax error.

Fig. 3. Parallax distribution of Gaia EDR3 stars.

Photometry. Gaia uses its own photometric system [11]. The bandwidths are shown in Fig. 5.[1] They are not at all similar to Johnson's *UBV* scale [12] or to the Hipparcos/Tycho system [13]. The blue component of G_{BP} covers the area from near ultraviolet to red, and the red G_{RP}, from red to infrared. This system is distinguished from the *UBV* scale not only by the other boundaries of the band ranges but also by their width. The peaks of the Johnson scale are much narrower and do not overlap. The connection of the Gaia photomet-

ric scale with other similar systems will be established later [14].

Almost all stars have magnitude G (only five million do not have it), while just over 1.5 billion stars have the photometric magnitudes Bp (blue photometer) and Rp (red photometer) (270 million do not).

The catalog contains the measured fluxes of photons in three bands and their errors, but there are no errors of the stellar magnitudes themselves, since stellar magnitudes are related in a nonlinear way with the measured flux [9].

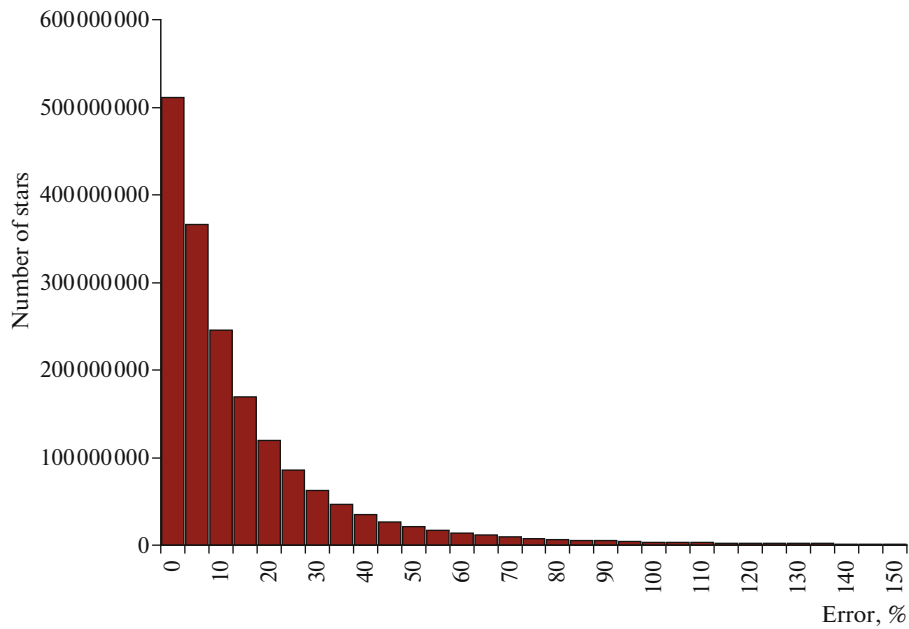Figure 6 shows the distribution of Gaia stars by magnitude G. The maximum distribution is at magnitude 20.

---

[1] The journal *Vestnik RAN* (the Russian version of *Herald of the RAS*) with color images is placed in the public domain on the website of the IKTs Akademkniga https://sciencejournals.ru/journal/vestnik/. Registration is not required to access the full texts of the journal.

Fig. 4. Distribution of Gaia EDR3 stars by the relative error of total proper motion.

DISTRIBUTION OF STARS IN THE CELESTIAL SPHERE

Stellar density vs. G. The distribution of stars in the catalog over the celestial sphere shows that, even for bright stars ($G = 8$), concentration towards the galactic equator is clearly observed. This suggests that there are already distant objects among them. For fainter stars ($G = 20$), the concentration is seen towards the galactic plane and bulge—the main observed effect (Fig. 7). To represent the stellar density, the celestial sphere was
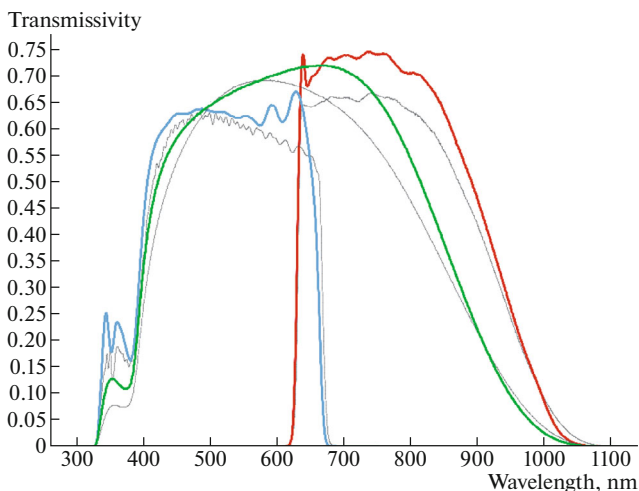

Fig. 5. Gaia EDR3 bandwidths. The colored lines in the figure show the G (green), Bp (blue), and Rp (red) bandwidths defining the Gaia EDR3 photometric system.

divided by the HealPix method [15] with the key number $N = 64$, which yielded 49 152 sites. Thus, one site occupied a little less than 1 square degree, more precisely, 0.83. The above illustrations may give the wrong impression that there are practically no stars in the circumpolar regions, but this is not so. Even far from the galactic equator, their density is hundreds of stars per square degree. It is clear that faint stars located far from the galactic equator are mostly nearby dwarfs.

Stellar density vs. distance to stars. The dependence of the distribution of stars over the celestial sphere on distance appears odd. If the relative accuracy of determining parallaxes is set better than 100% (the parallax is greater than the error), then even for nearby stars, to which the distance, according to Gaia, is less than 200 pc, a distinct concentration is observed towards the galactic equator (Fig. 8). Moreover, even the Magellanic Clouds are clearly visible. The picture for nearby stars does not differ much from the distribution of stars with distances from 800 pc to 1 kpc (Fig. 9), and even this distribution, in which the bulge of the Galaxy is visible, is rather typical for very distant stars (several kpc). A similar character is retained for stars of other distances. This leads to speculation about the unreliability of parallaxes (even in statistical terms) for the closest stars, where we can expect a high relative accuracy of parallaxes due to their location.

However, if we restrict ourselves to stars for which the parallax is determined with an accuracy of 10% or better, then the picture changes. The only strange result is the five closest stars where their concentration is still observed towards the equator. For other dis-
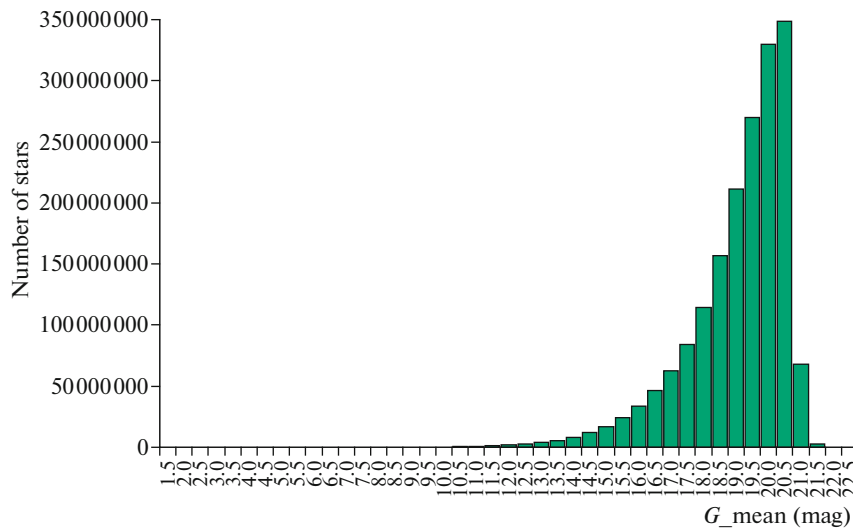
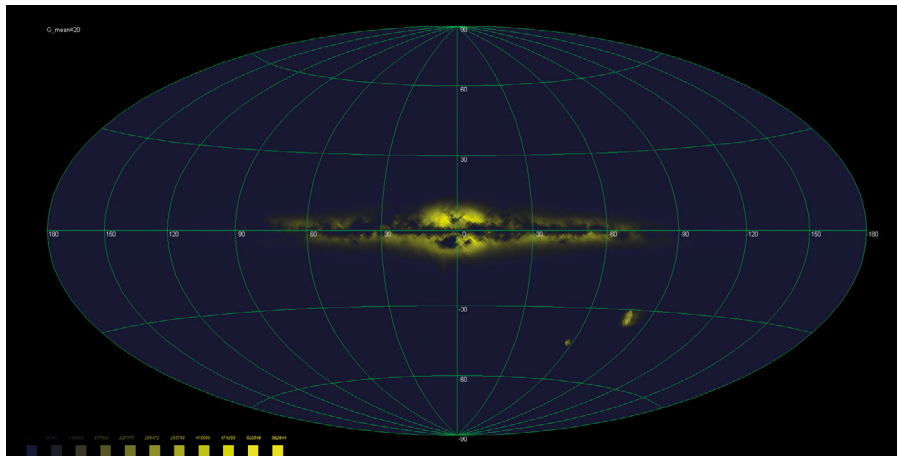**Fig. 6.** Distribution of Gaia EDR3 stars by magnitude G.

Fig. 7. Distribution of Gaia DR3 over the celestial sphere for stars with G = 20^m (maximum density is about 600 000 stars per pixel; 1 pixel = 0.83 sq. degrees).

tances, the picture is more predictable. Stars closer to 1 kpc are more evenly distributed over the celestial sphere, although, of course, their concentration can be traced to the galactic disk (Fig. 10). Distant stars clearly show the disk of the Galaxy (Fig. 11).

The distribution of the average color of the stars. It is very interesting to study the distribution of the average color index of stars *Bp−G* for different points of the celestial sphere (Fig. 12). In this case, to build the most detailed high-resolution image (the number of stars allows it), we abandoned the HealPix sites. Instead, we just used image pixels. The image itself has a size of 2000 × 1000 pixels. Even a cursory glance leads to the conclusion that there is a "reddening" of the color of the stars, caused by dusty matter. The fibrous structure of gas and dust clouds is clearly visible. A similar picture is observed for other color indicators. Obviously,

dust clouds not only cause reddening, but also significantly weaken the light of stars, which should be taken into account when conducting studies in which the stellar or absolute stellar magnitude will appear.

Closer attention to the polar regions shows that, first, there is almost no dusty matter in this direction, and second, in the polar regions one can see stars with a high (two or more) or low (0.5−0.7) color index. Most likely, these are nearby main sequence stars and white dwarfs.

The celestial sphere in a quasi-color image. Three-color photometry makes it possible to construct pseudo-color images of the celestial sphere, which have not only cognitive but also aesthetic value. Indeed, let us translate the photometric scale Bp, G, and Rp into the RGB scale used in computer images, and we will clearly see (Fig. 13) how light is absorbed
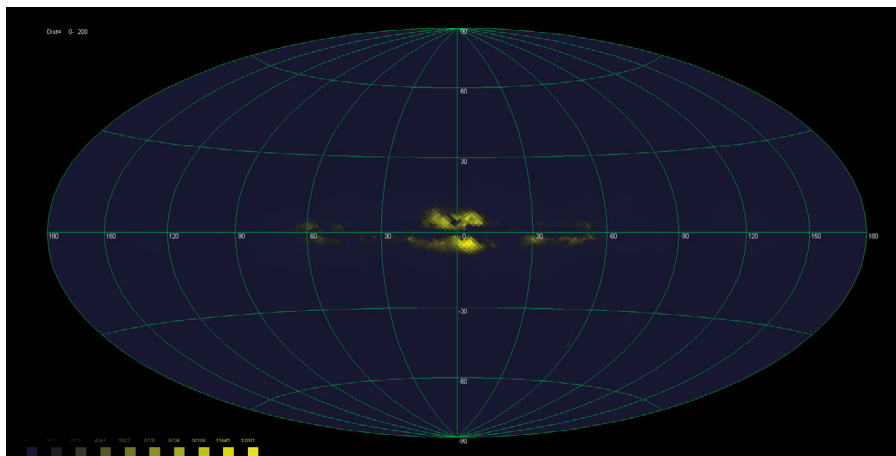
Fig. 8. Gaia DR3 distribution over the celestial sphere for stars with distances (relative accuracy of parallaxes <100%) from 0 to 200 pc (maximum density is about 13 000 stars per pixel; 1 pixel = 0.83 square degrees).
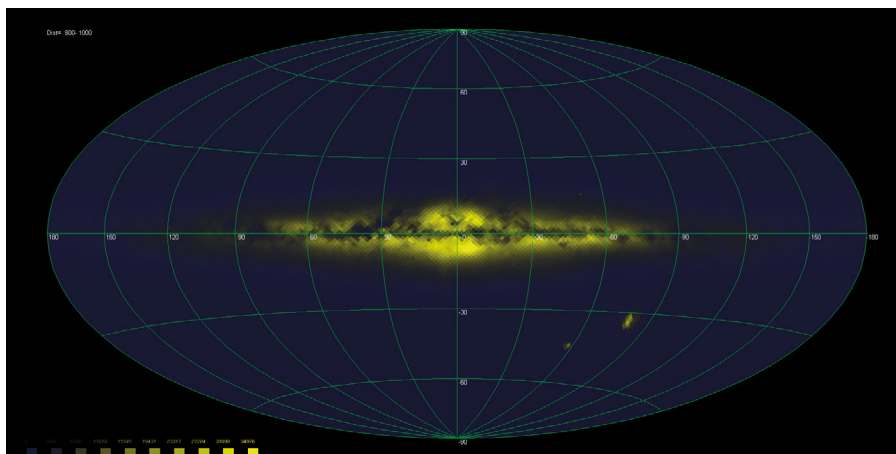
Fig. 9. Gaia DR3 distribution over the celestial sphere for stars with distances (relative accuracy of parallaxes <100%) from 800 to 1000 pc (maximum density is about 34 000 stars per pixel; 1 pixel = 0.83 square degrees).
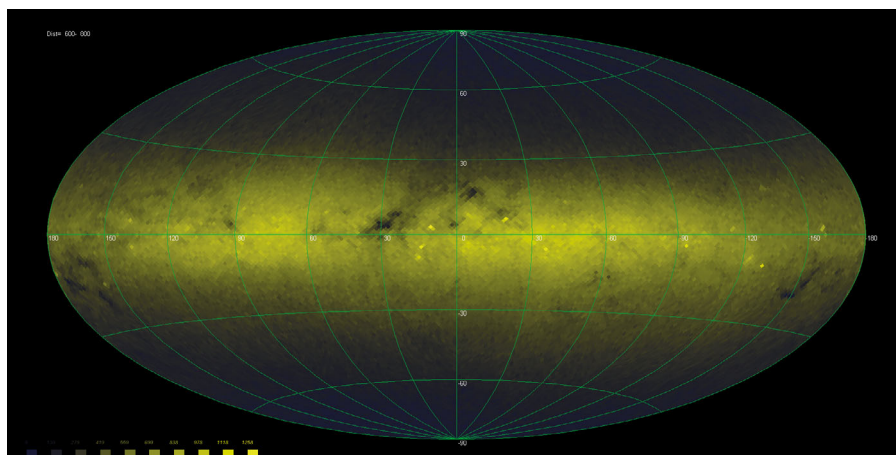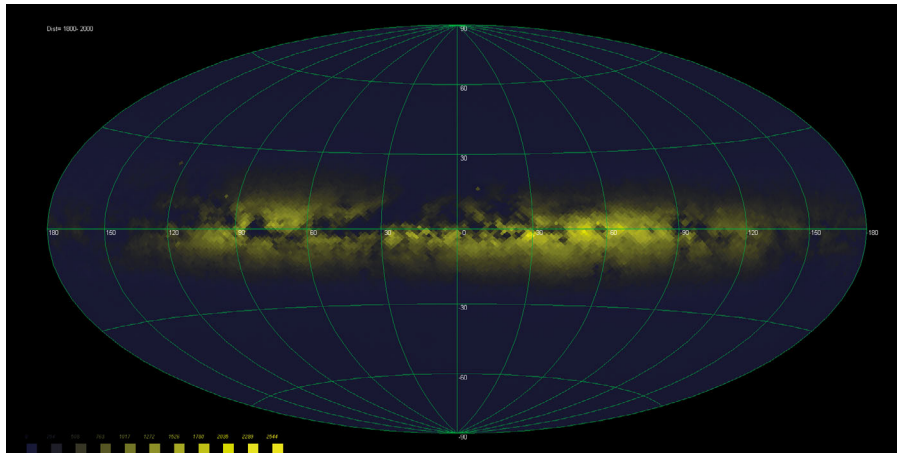

Fig. 10. Gaia DR3 distribution over the celestial sphere for stars with distances (relative accuracy of parallaxes <10%) from 600 to 800 pc (maximum density is about 1200 stars per pixel; 1 pixel = 0.83 square degrees).

Fig. 11. Distribution of Gaia DR3 over the celestial sphere for stars with distances (relative accuracy of parallaxes <10%) from 1.8 to 2.0 kpc (maximum density is about 2500 stars per pixel; 1 pixel = 0.83 square degrees).
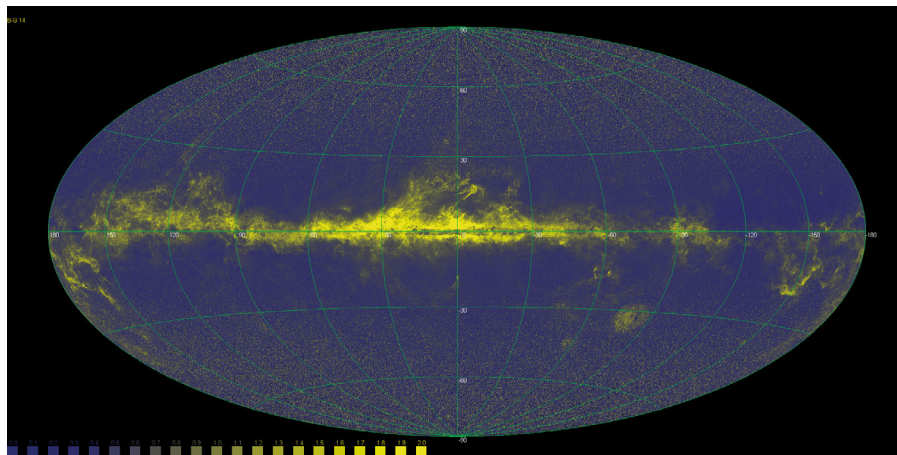
Fig. 12. The value of the average Bp−G color index of the Gaia DR3 stars of the 14th magnitude G depending on the position on the celestial sphere (blue corresponds to a value of 0.0, yellow corresponds to a value of 2.0).
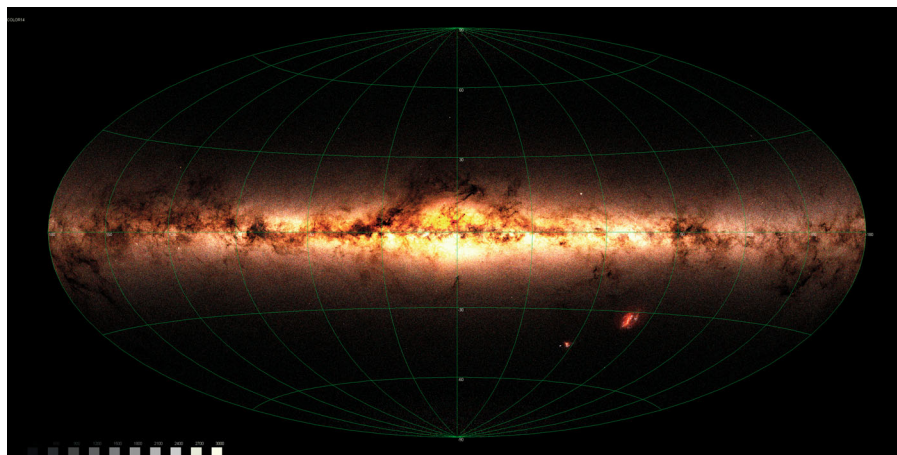
Fig. 13. Pseudo-color image of Gaia DR3 14 stars of magnitude G.
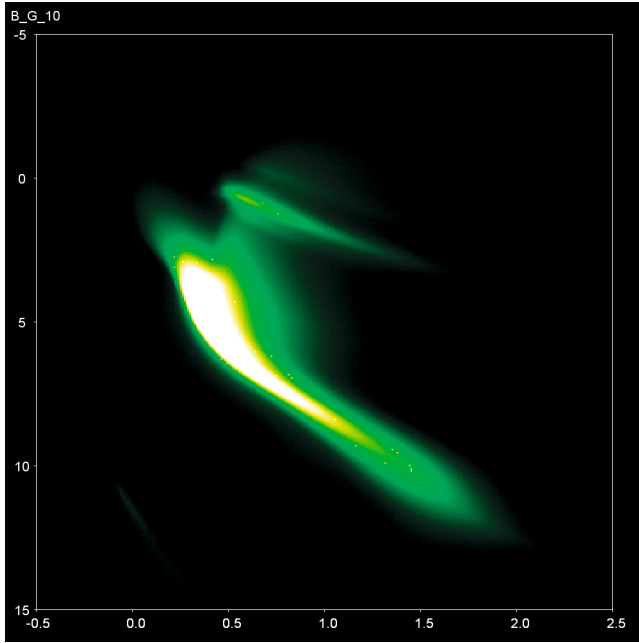
Fig. 14. Diagram "Bp−G color index−absolute stellar magnitude G" for stars with a relative parallax accuracy better than 10%.

in dusty clouds and how stars of different spectral classes are distributed over the celestial sphere.

HERTZSPRUNG−RUSSELL DIAGRAMS

The presence of distances and multicolor photometry makes it possible to construct a Hertzsprung−Russell diagram, more precisely, the diagram "color index−absolute magnitude." One can select $Bp−G$, $Bp−Rp$, or $G−Rp$ as the color index. The relationship with the standard color index $B−V$ has not yet been finally calibrated [16]. The use of stars with different parallax accuracy radically changes the whole picture. Indeed, if the parallax accuracy is set to 10% or better, then the diagram (Fig. 14) perfectly distinguishes all the main sequences and even subsequences. In addition to the main sequence, the branch of red giants and subgiants is clearly visible. In the lower left-hand corner, there is a rather thin area of white dwarfs. The image is built in conventional colors: the green color of maximum intensity corresponds to 250 stars hitting a pixel of 0.04^m in absolute magnitude and 0.01^m in the color index, yellow is about 500, and white is over 750 stars.

When going to stars with a parallax accuracy better than 50%, the picture is blurred. The main effect is the displacement of the stars downward, towards an increase in the absolute stellar magnitude, that is, a decrease in luminosity. In fact, brighter stars are located at large distances, and the Gaia parallaxes are shifted upward; in other words, the distances to the stars are underestimated. This is confirmed by the distribution of nearby stars in the celestial sphere, which are actually distant and therefore concentrate towards the galactic equator.

PROPER STAR MOTIONS

Behavior of the proper motions of stars of different sizes. The Gaia catalog contains only the equatorial proper motions of the stars $\mu_\alpha \cos \delta$ and μ_δ. For stellar kinematic studies, it is not difficult to translate them into galactic $\mu_l \cos b$ and μ_b:

$$\begin{aligned} \mu_l \cos b = & \quad \cos(\varphi)\mu_\alpha \cos \delta + \sin(\varphi)\mu_\delta, \\ \mu_b = & -\sin(\varphi)\mu_\alpha \cos \delta + \cos(\varphi)\mu_\delta, \end{aligned} \quad (1)$$

where

$$\begin{aligned} \sin \varphi &= \frac{\sin i \cos (l - L_0)}{\cos \delta}, \\ \cos \varphi &= \frac{\cos b \cos i - \sin b \sin i \sin (l - L_0)}{\cos \delta}. \end{aligned} \quad (2)$$

Here, i is the tilt angle of the galactic equator (62.87° at J 2000), and L_0 is the difference in longitudes between the direction to the center of the Galaxy and the intersection of the celestial and galactic equators (32.93°). Since these values are often used when generating binary files from a text directory, they can be immediately counted and written in order to save computational time in the future.

Before evaluating the stellar kinematic parameters, let us look at the behavior of proper motions depending on the stellar magnitude used. For proper motions in longitude (Figs. 15, 16) and latitude (Figs. 17, 18), it can be seen that bright stars ($G = 10$) have a combined picture, there are various kinematic effects, while for faint stars ($G = 20$), obviously, only general global kinematic effects remain, such as the rotation of the Galaxy.

Parameters of the standard stellar kinematic model. As the first, we use the well-known Ogorodnikov−Milne model [17]; a detailed form of the equations of this model is also presented in [18, 19]. In this model, the stellar velocity field is represented by the linear expression

$$\mathbf{V} = \mathbf{V}_0 + \Omega \times \mathbf{r} + \mathbf{M}^+ \times \mathbf{r}, \quad (3)$$

where V is the star speed; V_0 is the influence of the translational motion of the Sun; Ω is the angular velocity of the solid-body rotation of the stellar system; and $\mathbf{M}^+$ is the symmetric strain tensor of the velocity field.

The model contains 12 parameters, but not all of them can be determined independently from the proper motions, and not all parameters are included in the radial velocity equations:

U, V, W are components of the vector V_0 of the translational motion of the Sun among the stars;
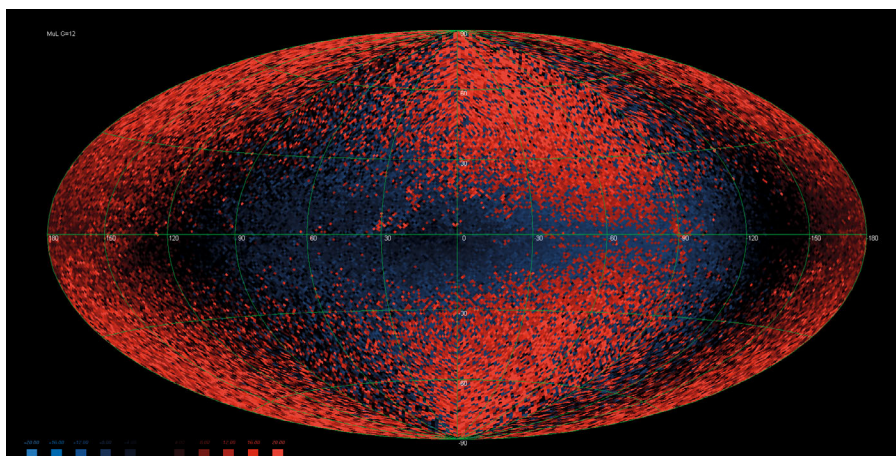
Fig. 15. Behavior of proper motions $\mu_l \cos b$ for stars G = 12 (from −20 to +20 mas/yr).
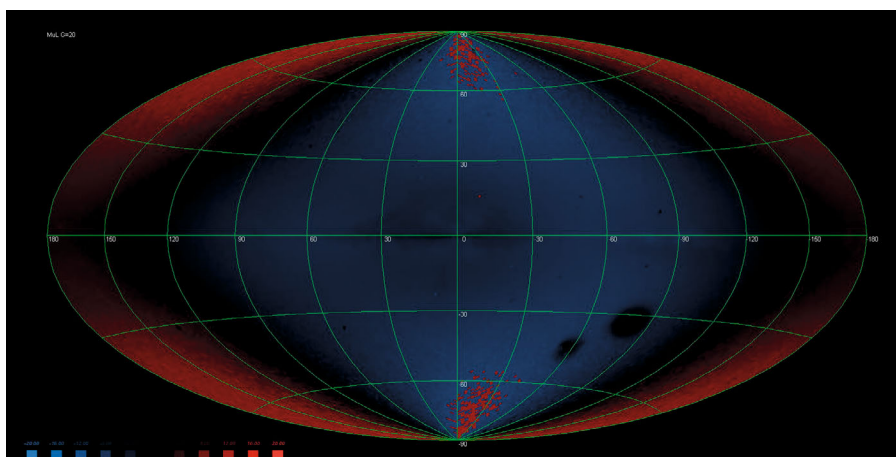
Fig. 16. Behavior of proper motions $\mu_l \cos b$ for stars G = 20 (from −20 to +20 mas/yr).
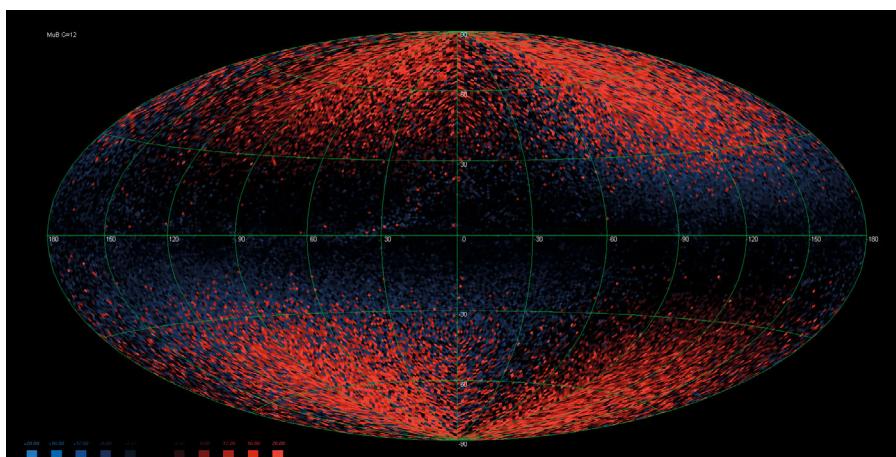
Fig. 17. Behavior of proper motions μ_b for stars G = 12 (from −20 to +20 mas/yr).
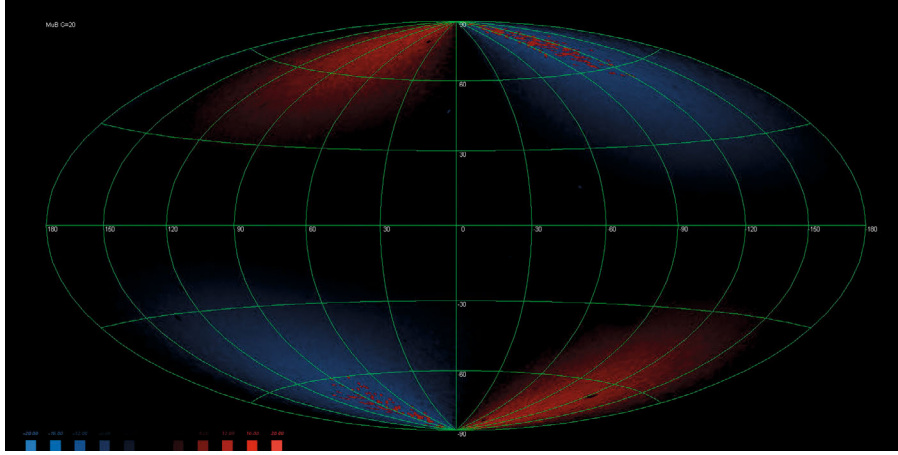
Fig. 18. Behavior of proper motions μ_b for stars G = 20 (from −20 to +20 mas/yr).

ω_1, ω_2, ω_3 are components of the angular velocity vector $\mathbf{\Omega}$;

$M_{11}^+, M_{22}^+, M_{33}^+$ are the strain tensor parameters describing compression–tension along the principal axes of the galactic coordinate system;

$M_{12}^+, M_{13}^+, M_{23}^+$ are the parameters of tensor $\mathbf{M}^+$, describing the deformation of the velocity field in the main plane and two perpendicular planes.

By projecting Eq. (3) onto the unit vectors of the galactic coordinate system, we obtain

$$
\begin{aligned}
k\mu_l \cos b = &\, U/r \sin l - V/r \cos l - \omega_1 \sin b \cos l \\
&- \omega_2 \sin b \sin l + \omega_3 \cos b + M_{12}^+ \cos b \cos 2l \\
&- M_{13}^+ \sin b \sin l + M_{23}^+ \sin b \cos l \\
&- \frac{1}{2} M_{11}^+ \cos b \sin 2l + \frac{1}{2} M_{22}^+ \cos b \sin 2l,
\end{aligned} \tag{4}
$$

$$
\begin{aligned}
k\mu_b = &\, U/r \cos l \sin b + V/r \sin l \sin b \\
&- W/r \cos b + \omega_1 \sin l - \omega_2 \cos l \\
&- \frac{1}{2} M_{12}^+ \sin 2b \sin 2l + M_{13}^+ \cos 2b \cos l \\
&+ M_{23}^+ \cos 2b \sin l - \frac{1}{2} M_{11}^+ \sin 2b \cos^2 l \\
&- \frac{1}{2} M_{22}^+ \sin 2b \sin^2 l + \frac{1}{2} M_{33}^+ \sin 2b.
\end{aligned} \tag{5}
$$

In formulas (4) and (5), there is a linear relationship between the coefficients $M_{11}^+, M_{22}^+, M_{33}^+$; therefore, when analyzing proper motions, the authors usually introduce the substitutions $M_{11}^* = M_{11}^+ - M_{22}^+$ and $M_{33}^* = M_{33}^+ - M_{22}^+$ [18], or [20], and instead of M_{33}^*, they introduce the value

$$
X = M_{33}^+ - \frac{M_{11}^+ + M_{22}^+}{2}. \tag{6}
$$

In this case, Eqs. (4) and (5) are rewritten as

$$
\begin{aligned}
k\mu_l \cos b = &\, U/r \sin l - V/r \cos l - \omega_1 \sin b \cos l \\
&- \omega_2 \sin b \sin l + \omega_3 \cos b + M_{12}^+ \cos b \cos 2l \\
&- M_{13}^+ \sin b \sin l + M_{23}^+ \sin b \cos l \\
&- \frac{1}{2} M_{11}^* \cos b \sin 2l,
\end{aligned} \tag{7}
$$

$$
\begin{aligned}
k\mu_b = &\, U/r \cos l \sin b + V/r \sin l \sin b \\
&- W/r \cos b + \omega_1 \sin l - \omega_2 \cos l \\
&- \frac{1}{2} M_{12}^+ \sin 2b \sin 2l + M_{13}^+ \cos 2b \cos l \\
&+ M_{23}^+ \cos 2b \sin l \\
&- \frac{1}{4} M_{11}^* \sin 2b \cos 2l + \frac{1}{2} X \sin 2b.
\end{aligned} \tag{8}
$$

Equations (7) and (8) are often used to solve jointly the total proper motions of some catalog, and if the distance to the stars is unknown, then, instead of the quantities U, V, W, $U/\langle r \rangle$, $V/\langle r \rangle$, $W/\langle r \rangle$ are determined, where $\langle r \rangle$ is the average distance of the sample of stars for which the solution is made.

Tables 1 and 2 show the joint solution for Gaia EDR3 stars, and the graphs in Figs. 19−21 illustrate the data in the tables.

Analysis of these results shows that the solar terms $U/\langle r \rangle$, $V/\langle r \rangle$, $W/\langle r \rangle$, as expected, decrease with increasing stellar magnitude, since there is a complete correlation between the brightness of the star and the distance. The largest component is the movement of the Sun along the axis $Y - V/\langle r \rangle$. For bright stars of magnitude 3−6, these parameters are determined

Table 1. The values of the components of the velocity of the Sun's motion and the angular velocity of solid rotation in km/s/kpc, obtained from the joint solution for stars of different G values

G	$U/\langle r \rangle$	$V/\langle r \rangle$	$W/\langle r \rangle$	ω_1	ω_2	ω_3
3	158.1 ± 44.5	294.2 ± 45.4	159.4 ± 42.5	45.6 ± 45.2	19.4 ± 45.7	-26.4 ± 42.3
4	184.9 ± 31.3	209.2 ± 32.0	128.1 ± 29.3	-59.5 ± 32.2	25.8 ± 32.6	3.6 ± 29.3
5	116.5 ± 10.6	181.0 ± 10.7	71.5 ± 9.9	-13.1 ± 10.8	13.2 ± 10.9	-21.1 ± 9.8
6	75.0 ± 4.9	132.3 ± 5.0	50.7 ± 4.5	6.1 ± 5.0	8.2 ± 5.1	-15.6 ± 4.5
7	59.6 ± 1.9	111.2 ± 1.9	38.4 ± 1.8	1.9 ± 1.9	-7.5 ± 2.0	-12.2 ± 1.8
8	44.8 ± 1.0	91.3 ± 1.0	30.4 ± 1.0	0.6 ± 1.0	-4.9 ± 1.0	-11.4 ± 1.0
9	35.0 ± 0.6	77.7 ± 0.6	25.2 ± 0.6	1.5 ± 0.6	-4.4 ± 0.6	-10.7 ± 0.6
10	30.1 ± 0.3	67.1 ± 0.3	19.5 ± 0.3	0.6 ± 0.3	-2.8 ± 0.3	-11.6 ± 0.3
11	24.9 ± 0.2	58.8 ± 0.2	15.9 ± 0.2	0.8 ± 0.2	-2.4 ± 0.2	-11.8 ± 0.2
12	20.6 ± 0.1	51.6 ± 0.1	13.1 ± 0.1	0.2 ± 0.1	-2.0 ± 0.1	-11.9 ± 0.1
13	17.3 ± 0.1	46.3 ± 0.1	10.7 ± 0.1	0.3 ± 0.1	-1.1 ± 0.1	-12.4 ± 0.1
14	14.9 ± 0.1	42.5 ± 0.1	8.8 ± 0.1	0.4 ± 0.1	-0.9 ± 0.1	-12.8 ± 0.1
15	12.7 ± 0.1	39.8 ± 0.1	7.3 ± 0.1	0.5 ± 0.1	-0.7 ± 0.1	-12.9 ± 0.1
16	10.9 ± 0.1	38.1 ± 0.1	6.3 ± 0.1	0.6 ± 0.1	-0.7 ± 0.1	-12.6 ± 0.1
17	9.6 ± 0.0	36.9 ± 0.0	5.5 ± 0.0	0.6 ± 0.0	-0.7 ± 0.0	-12.3 ± 0.0
18	8.4 ± 0.0	35.5 ± 0.0	4.9 ± 0.0	0.4 ± 0.0	-0.6 ± 0.0	-12.1 ± 0.0
19	7.2 ± 0.0	33.2 ± 0.0	4.4 ± 0.0	0.2 ± 0.0	-0.5 ± 0.0	-11.9 ± 0.0
20	6.5 ± 0.0	31.7 ± 0.0	4.2 ± 0.0	0.3 ± 0.0	-0.5 ± 0.0	-11.8 ± 0.0

unreliably; this is also true for other parameters. The reason is not only a small number of stars in this range (they are still not so few for equations with 11 parameters) but also the peculiar kinematics of nearby stars.

Researchers have been paying attention to this since the 1950s [21].

Considering such an important parameter as the angular velocity of the solid-body rotation of the sys-
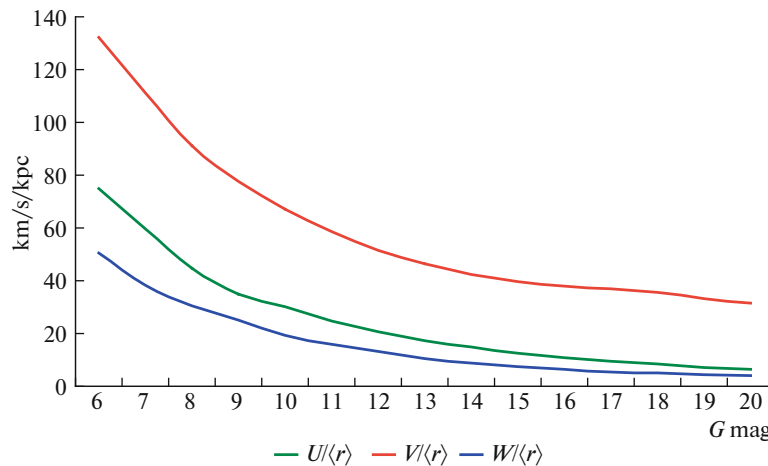

Fig. 19. Dependence of the kinematic parameters of the Sun's motion $U/\langle r \rangle$, $V/\langle r \rangle$, $W/\langle r \rangle$ on the stellar magnitude (km/s/kpc).

Table 2. Values of the strain tensor components in km/s/kpc obtained from the joint solution for stars of different G values

G	M_{12}	M_{13}	M_{23}	M_{11}^*	X
3	-36.1 ± 55.2	18.3 ± 58.1	-126.9 ± 57.1	192.9 ± 110.8	1.1 ± 103.8
4	-1.8 ± 37.8	4.1 ± 41.5	28.3 ± 39.6	-127.3 ± 78.5	37.2 ± 74.8
5	15.1 ± 13.0	9.3 ± 13.7	2.1 ± 13.5	6.9 ± 25.9	-39.9 ± 25.1
6	25.2 ± 6.0	17.1 ± 6.4	-5.0 ± 6.3	1.3 ± 11.9	8.9 ± 11.6
7	14.6 ± 2.3	-3.3 ± 2.5	-3.4 ± 2.4	2.8 ± 4.6	-7.0 ± 4.4
8	15.2 ± 1.3	-2.3 ± 1.3	-2.9 ± 1.3	-3.0 ± 2.5	-2.1 ± 2.3
9	15.6 ± 0.8	-1.9 ± 0.8	-1.9 ± 0.8	-1.2 ± 1.6	1.6 ± 1.4
10	17.1 ± 0.4	-0.9 ± 0.4	-1.1 ± 0.4	-0.3 ± 0.9	-0.7 ± 0.7
11	15.9 ± 0.2	-0.5 ± 0.2	-1.3 ± 0.2	-1.3 ± 0.5	1.3 ± 0.4
12	15.2 ± 0.2	-0.5 ± 0.2	-0.4 ± 0.2	-1.2 ± 0.3	0.6 ± 0.3
13	14.3 ± 0.1	-0.1 ± 0.1	-0.1 ± 0.1	-1.4 ± 0.2	1.4 ± 0.2
14	13.3 ± 0.1	-0.3 ± 0.1	-0.3 ± 0.1	-1.1 ± 0.2	1.0 ± 0.1
15	12.7 ± 0.1	-0.4 ± 0.1	-0.4 ± 0.1	-0.9 ± 0.1	0.9 ± 0.1
16	12.1 ± 0.1	-0.3 ± 0.1	-0.5 ± 0.1	-0.3 ± 0.1	0.5 ± 0.1
17	11.4 ± 0.1	-0.1 ± 0.1	-0.4 ± 0.1	0.1 ± 0.1	0.3 ± 0.1
18	10.2 ± 0.1	0.1 ± 0.1	-0.1 ± 0.1	0.4 ± 0.1	0.4 ± 0.1
19	9.1 ± 0.0	0.2 ± 0.0	0.0 ± 0.0	0.5 ± 0.1	0.6 ± 0.1
20	8.6 ± 0.0	0.1 ± 0.0	-0.1 ± 0.0	0.4 ± 0.1	0.6 ± 0.1

tem ω_1, ω_2, ω_3, we also see that, for the brightest stars, the parameters of the angular velocity vector are not determined at all, and, starting from the stars of magnitude 7, the vector is determined well and is not perpendicular to the plane of the Galaxy. This fact is also known [22]. The following circumstances are interesting. First, starting from stars of magnitude 12, the errors of the determined parameters become
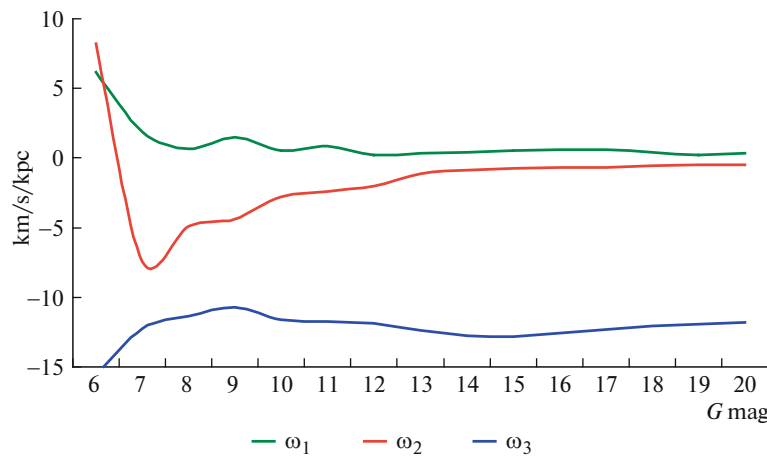
Fig. 20. Dependence of the angular velocity of solid rotation ω_1, ω_2, ω_3 on the stellar magnitude (km/s/kpc).
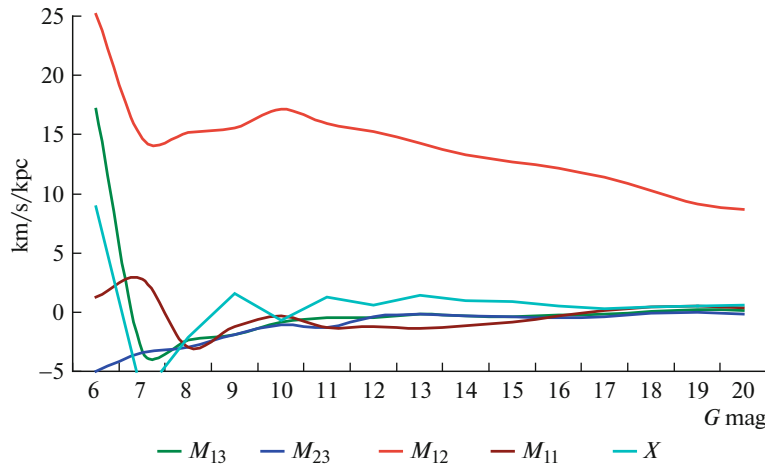
Fig. 21. Dependence of strain tensor components M_{12}, M_{13}, M_{23}, M_{11}^*, X on the stellar magnitude (km/s/kpc).

extremely small; that is, the peculiar velocities of the stars cease to play a significant role. Second, the components of the rotation vector ω_1 and ω_2 significantly differ from zero even for faint (and, apparently, distant) stars; this indicates that the rotation vector is not completely perpendicular to the galactic plane.

Analysis of the strain tensor components shows that practically all components, with the exception of the parameter M_{12} (and this is the Oort parameter A), decrease rapidly to zero values. An exception is the parameter M_{11}, responsible for the difference in the stretching of the star system along the axes X and Y. It retains a nonzero value for quite a long time, and decreases strongly only for stars of magnitude 16, 17, and fainter.

Dependence of the parameters of the standard stellar kinematic model on distances. Analysis of the distributions of stars in terms of parallaxes and their accuracies shows that stars with a high relative accuracy of parallaxes should be used for stellar kinematic studies that require distances. For this we have created a subcatalog of 98 506 335 stars that meet this criterion. The size of the binary file was only 14 GB (compared to 260 for the full catalog). Accordingly, the speed of working with this data has increased almost 20 times. Since even a 10% parallax accuracy still does not guarantee the true parallax value of each star, we acted in the standard way, breaking the stellar material into spherical layers remote from the Sun at different distances. For these groups of stars, the equations were solved in the framework of the Ogorodnikov−Milne model and the proper motions were expanded in terms of a system of vector spherical functions. The results are shown in Tables 3 and 4. For compactness, the distances, starting at 400 pc, are not given in succession, since the values change slowly. Full versions of the tables are contained in the electronic Appendix

(http://school.podvorye.ru/astro/GAIA_EDR3/). Table 4 additionally shows the number of stars used in the solution. The solution itself was based on the averaged data of proper motions and distances over 49 152 HealPix sites ($N = 64$) with their equal weights. Figures 22−24 illustrate the contents of Tables 3 and 4.

Analysis of the results shows that, within 1.5−2 kpc, the three-dimensional model is able to describe the kinematics of stars satisfactorily, although the parameters themselves sometimes undergo significant changes depending on the group of stars under consideration (especially the solar parameter V). As before, the closest stars constitute a problem area in which the kinematics does not obey the three-dimensional model. However, from a distance of about 300 pc, the kinematic parameters take their usual values. Stars closer than 100 pc have high peculiar velocities, which simply cease to be noticeable with distance, since the global rotation effects of the Galaxy increase.

Generally speaking, it is believed that the simplified linear Oort−Lindblad model or the complete Ogorodnikov−Milne model can be used up to distances of 1−1.5 kpc [17]. However, we see that, in principle, the Oort parameters $A = M_{12}$ and $B = \omega_3$, although they change with distance very smoothly, still retain their general character. Other parameters— such as components of angular velocity ω_1 and ω_2, as well as of strain tensor M_{11}^*, M_{13}, M_{23}, X—tend to values close to zero with increasing distance. Only M_{11}^* shows zero values (the difference in compression of the system along the X and Y axes).

Most striking is the variation of the parameter V— the speed of the Sun along the Y axis, directed along the rotation of the Galaxy. The explanation can probably be given as follows: the speed of the Sun is estimated relative to groups of stars at different distances,

Table 3. The values of the components of the speed of the Sun's motion in km/s and the angular velocity of solid rotation in km/s/kpc, obtained from the joint solution for stars of different distances

r	U	V	W	ω_1	ω_2	ω_3
0−100	10.2 ± 0.1	22.0 ± 0.1	7.2 ± 0.1	-1.1 ± 1.4	-12.1 ± 1.4	-1.5 ± 1.4
100−200	9.7 ± 0.0	23.2 ± 0.0	7.3 ± 0.0	1.2 ± 0.2	-6.3 ± 0.2	-10.1 ± 0.2
200−300	9.9 ± 0.0	24.7 ± 0.0	7.7 ± 0.0	1.1 ± 0.1	-2.5 ± 0.1	-12.5 ± 0.1
300−400	10.3 ± 0.0	25.8 ± 0.0	7.8 ± 0.0	0.8 ± 0.1	-1.3 ± 0.1	-13.0 ± 0.1
500−600	10.8 ± 0.0	27.7 ± 0.0	7.8 ± 0.0	1.0 ± 0.0	-1.1 ± 0.0	-13.7 ± 0.0
700−800	11.5 ± 0.0	30.7 ± 0.0	7.8 ± 0.0	-0.1 ± 0.0	-0.4 ± 0.0	-13.7 ± 0.0
900−1K	12.1 ± 0.0	34.6 ± 0.0	8.0 ± 0.0	0.1 ± 0.0	0.2 ± 0.0	-13.7 ± 0.0
1.2−1.3K	12.9 ± 0.1	40.5 ± 0.1	8.0 ± 0.1	0.7 ± 0.0	0.5 ± 0.0	-13.8 ± 0.0
1.5−1.6K	13.4 ± 0.1	46.5 ± 0.1	8.1 ± 0.1	1.2 ± 0.1	0.4 ± 0.1	-14.0 ± 0.1
1.8−1.9K	13.4 ± 0.1	52.4 ± 0.1	8.0 ± 0.1	1.2 ± 0.1	0.4 ± 0.1	-14.2 ± 0.1
2.1−2.2	13.5 ± 0.2	58.2 ± 0.2	8.0 ± 0.2	1.2 ± 0.1	0.3 ± 0.1	-14.5 ± 0.1
2.4−2.5	13.9 ± 0.2	62.2 ± 0.2	7.8 ± 0.2	0.0 ± 0.1	0.0 ± 0.1	-14.9 ± 0.1

Table 4. The values of the strain tensor components in km/s/kpc obtained from the joint solution for stars of different distances, as well as the number of stars participating in the solution

| r	M_{12}	M_{13}	M_{23}	M_{11}^*	X	N
0−100	28.0 ± 1.8	4.2 ± 1.8	-2.4 ± 1.8	-1.7 ± 3.6	0.1 ± 3.6	372226
100−200	19.4 ± 0.3	-1.3 ± 0.3	-1.2 ± 0.3	-2.3 ± 0.5	0.1 ± 0.5	1862090
200−300	15.7 ± 0.1	-0.7 ± 0.1	-0.8 ± 0.1	-5.1 ± 0.2	1.6 ± 0.2	3515477
300−400	14.7 ± 0.1	-0.5 ± 0.1	-0.3 ± 0.1	-5.9 ± 0.2	2.2 ± 0.1	4696935
500−600	14.5 ± 0.1	-1.1 ± 0.1	-0.6 ± 0.1	-6.5 ± 0.1	2.1 ± 0.1	5245459
700−800	14.1 ± 0.1	-0.4 ± 0.1	0.8 ± 0.1	-5.3 ± 0.1	2.1 ± 0.1	5272993
900−1K	13.5 ± 0.1	-0.1 ± 0.1	0.3 ± 0.1	-4.1 ± 0.1	1.8 ± 0.1	5235217
1.2−1.3K	12.8 ± 0.1	-0.1 ± 0.1	-0.6 ± 0.1	-3.4 ± 0.1	1.2 ± 0.1	4741504
1.5−1.6K	12.4 ± 0.1	-0.2 ± 0.1	-1.1 ± 0.1	-3.0 ± 0.1	1.4 ± 0.1	3871940
1.8−1.9K	11.8 ± 0.1	-0.3 ± 0.1	-1.2 ± 0.1	-2.8 ± 0.2	1.4 ± 0.1	2839861
2.1−2.2	11.1 ± 0.1	-0.4 ± 0.1	-1.2 ± 0.1	-2.5 ± 0.2	1.2 ± 0.1	1655812
2.4−2.5	10.3 ± 0.1	-0.7 ± 0.1	-0.5 ± 0.1	-2.4 ± 0.2	1.2 ± 0.2	1041495
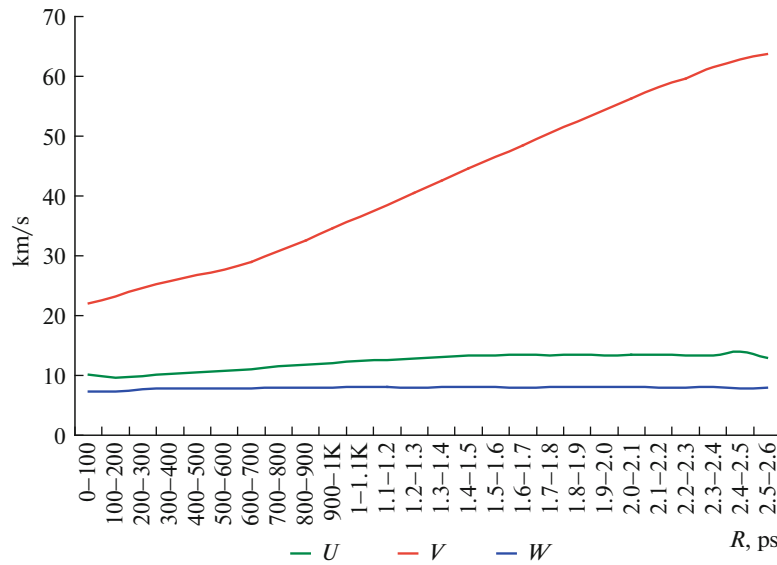
Fig. 22. Dependence of the kinematic parameters of the Sun's motion U, V, W on the distance to the stars (km/s).
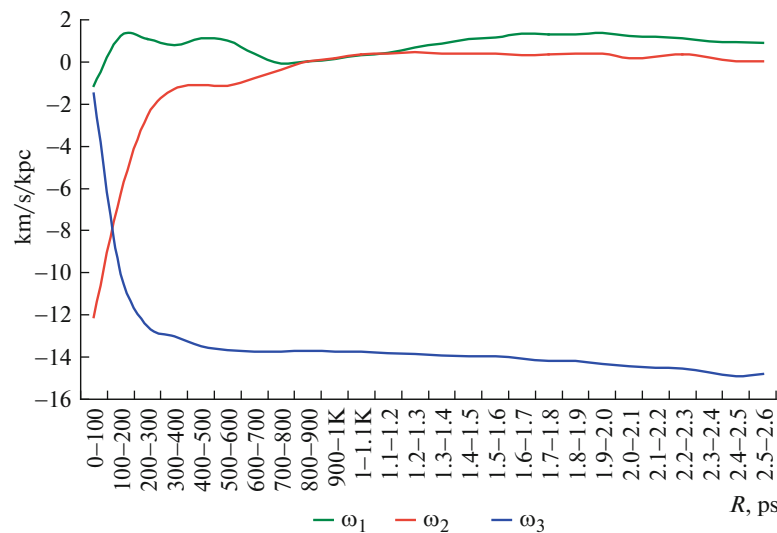

Fig. 23. Dependence of the angular velocity of solid rotation ω_1, ω_2, ω_3 on the distance to stars (km/s/kpc).

and these groups themselves move relative to each other, in the plane of the Galaxy in a direction perpendicular to its center. These differences are strong and have a large systematic course. We previously obtained similar results from the Gaia DR2 with RV catalog [22], but the behavior of the parameter V was somewhat different. Its value remained stable (about 22 km/s) up to distances of 800 pc, and then linear growth began. In our case, we immediately observe linear growth.

Another feature of the parameters of the Sun's motion is their reliable and predictable values even for the closest stars, which cannot be said about the parameters of rotation and deformation, which reach stable values only at distances of 400–500 pc.

* * *

This work is preparatory in nature with an eye to processing more accurate (especially in parallaxes) data of the final versions of the Gaia catalog, which will become available in early 2022. Nevertheless, even this material provides rich ground for various statistical and kinematic estimates of the catalog as a whole.
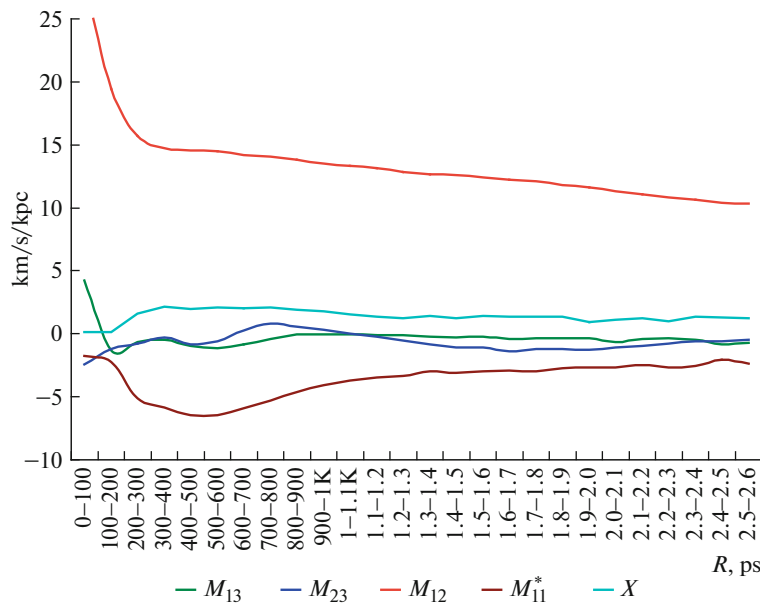
Fig. 24. Dependence of strain tensor components M_{12}, M_{13}, M_{23}, M_{11}^*, X on the distance to stars (km/s/kpc).

CONFLICT OF INTEREST

The author declares that he has no conflict of interest.

SUPPLEMENTARY INFORMATION

Additional illustrative material can be obtained at the link https://disk.yandex.ru/d/H0aj0INDTPt30Q.

REFERENCES

1. ESA. Gaia. https://sci.esa.int/web/gaia.
2. ESA. Gaia Early Data Release 3. https://www.cosmos.esa.int/web/gaia/earlydr3.
3. Gaia Collaboration, "Gaia Early Data Release 3: Summary of the contents and survey properties," Astron. Astrophys. **649** (A1), 1−20 (2021).
4. D. Michalik, L. Lindegren, and Hobbs, "The Tycho-Gaia astrometric solution: How to get 2.5 million parallaxes with less than one year of Gaia data," Astron. Astrophys. **574** (A115), 1−8 (2015).
5. D. Katz, P. Sartoretti, M. Cropper, et al., "Gaia Data Release 2: Properties and validation of the radial velocities," Astron. Astrophys. **622** (A205), 1−19 (2019).
6. N. Zacharias, D. G. Monet, S. E. Levine, et al., "The Naval Observatory Merged Astrometric Dataset (NOMAD). American Astronomical Society 205th meeting," Bull. Am. Astron. Soc. **36**, 1418 (2004).
7. S. Roeser, M. Demleitner, and E. Schilbach, "The PPMXL catalog of positions and proper motions on the ICRS. Combining USNO-B1.0 and the Two Micron All Sky Survey (2MASS)," Astron. J. **139** (6), 2440−2447 (2010).
8. O. V. Barten'ev, *Modern Fortran,* 3rd ed. (DIALOG−MIFI, Moscow, 2000) [In Russian].
9. Gaia. Chapter 13. https://gea.esac.esa.int/archive/documentation/GEDR3/Gaia_archive/chap_datamodel/.
10. A. Brown, A. Vallenari, T. Prusti, et al., "Gaia Early Data Release 3: Summary of the contents and survey properties," Astron. Astrophys. **649** (A1), 20 (2021).
11. P. Montegriffo, F. De Angeli, M. Bellazzini, et al., GAIA EDR3 passbands. 2020. https://www.cosmos.esa.int/web/gaia/edr3-passbands.
12. H. L. Johnson and W. W. Morgan, "Fundamental stellar photometry for standards of spectral type on the Revised System of the Yerkes Spectral Atlas," Astrophys. J. **117** (3), 313−352 (1953).
13. A. S. Tsvetkov, *Hipparcos Directory Practical Guide* (Izd. SPbGU, St. Petersburg, 2005) [in Russian].
14. M. Riello, F. De Angeli, D. W. Evans, et al., "GAIA Early Data Release 3: Photometric content and validation," Astron. Astrophys. **649** (A3), 1−33 (2021).
15. K. M. Gorski, E. Hivon, A. J. Banday, et al., "HEALPix: A framework for high-resolution discretization and fast analysis of data distributed on the sphere," Astrophys. J. **622** (2), 759−771 (2005).
16. L. Casagrande and D. VandenBerg, "On the use of Gaia magnitudes and new tables of bolometric corrections," Mon. Not. of R. Astron. Soc.: Letters **479** (1), L102−L107 (2018).
17. K. F. Ogorodnikov, *Dynamics of Stellar Systems* (Fizmatgiz, Moscow, 1965) [in Russian].
18. B. A. du Mont, "A three-dimensional analysis of the kinematics of 512 FK4/FK4 Sup. stars," Astron. Astrophys. **61** (127), 127−132 (1977).
19. S. P. Rybka, "Kinematic analysis of red giant stars in the vicinity of the Sun," Kinemat. Fiz. Nebes. Tel **20** (5), 437−443 (2004).
20. V. V. Vityazev, A. V. Popov, A. S. Tsvetkov, et al., "Kimnematics of stars from the TGAS (Gaia DR1) catalogue," Astron. Lett. **44** (4), 236−247 (2018).
21. R. B. Shatsova, "Asymmetry of the Boss GC's own movements," Uch. Zap. LGU, No. 136, 115−165 (1950).
22. A. S. Tsvetkov and F. A. Amosov, "Kinematic parameters of the stellar velocity field within 3 kpc of the Sun based on the Gaia Data Release 2 with radical velocities catalogue," Astron. Lett. **45** (7), 462−473 (2019).

Translated by B. Alekseev